



ELSEVIER

Physica D 89 (1996) 368–380

PHYSICA D

Dynamics of penta–hepta defects in hexagonal patterns

Lev S. Tsimring

Institute for Nonlinear Science, University of California, San Diego, CA 92093-0402, USA

Received 10 January 1995; revised 13 June 1995; accepted 14 June 1995

Communicated by L. Kramer

Abstract

The bound state of two dislocations known as a penta–hepta defect (PHD) is a generic object in hexagonal patterns. Its motion provides an important mechanism of wavevector(s) selection. In this paper the structure and dynamics of penta–hepta defects in hexagonal patterns is studied in the framework of envelope equations. Analytical solution for phase field of moving PHD is found in the far field, which generalizes the static solution due to Pismen and Nepomnyashchy (1993). The mobility tensor of PHD is calculated using combined analytical and numerical approach. The results for the velocity of PHD climbing in slightly non-optimal hexagonal patterns are in good agreement with numerical simulations of amplitude equations. Interaction of penta–hepta defects in optimal hexagonal patterns is studied numerically.

Keywords: Pattern formation; Hexagonal patterns; Defects; Mobility

PACS: 47.20.Ky; 47.27.Te; 64.90.+b

1. Introduction

It is widely recognized that defects play an important role in the wavevector selection in nonequilibrium cellular patterns. Considerable effort has been devoted to analysis of the structure and dynamics of dislocations in roll patterns (see [1]). Dynamics of defects in more complicated composite patterns such as hexagonal patterns attracted less attention. A hexagonal pattern is formed as a superposition of three plane waves oriented at 120° with respect to each other. They appear naturally in a large variety of pattern-forming systems in fluid dynamics [2,3], optics [4], chemical kinetics [5], etc. The most generic defect in hexagonal pattern is so called penta–hepta defect (PHD) which is a bound state of two dislocations of opposite winding numbers on two different wave systems [2,6]. In the paper [7] we have demonstrated that the mechanism

which provides binding force is the synchronization of the phase fields in the bulk of the system so the resonant condition for phases can be fulfilled everywhere except the core of the defect. After the penta–hepta defect has been created from two dislocations attracted to each other, it stays immobile in an ideal hexagonal pattern. Meanwhile, observations of penta–hepta defects in non-Boussinesq Rayleigh–Bénard convection and in other systems demonstrate that PHDs in fact move slowly and eventually annihilate or disappear at the boundaries [8]. It is conceivable that the motion of PHDs is caused by interaction with each other and other imperfections of the real hexagonal patterns, in particular by detuning of wavenumbers of the underlying waves from the onset value. Recently, in a number of papers, such imperfect hexagonal patterns have been studied theoretically. In Refs. [9–11] stability limits of equilateral hexagons with non-optimal (but

equal) wavenumbers were found; in Refs. [12–14] non-equilateral (rhombic) patterns were investigated.

In this paper, we will focus on the motion of PHDs in non-optimal hexagonal patterns. The analysis will be carried in the framework of three coupled amplitude equations for complex amplitudes of individual waves. These equations constitute the simplest heuristic model for hexagonal patterns and play essentially the same role here as the complex Ginzburg–Landau equation for oscillatory media or the Newell–Whitehead–Segel equation for roll patterns in isotropic media.

In Section 2 we start from the amplitude equations and deduce the equations of motion of a PHD in a general form. These equations relate the velocity vector of the penta–hepta defect with corrections to the onset value of the wavenumber. Defect is driven by a linear superposition of *two* Peach–Köhler forces from individual modes, since only two singular modes (modes with dislocations) affect the defect motion in the first approximation. The velocity vector is related to the Peach–Köhler forces via a mobility tensor. The mobility tensor for the penta–hepta defect is calculated in Section 3. In the core region, stationary numerical solution of 2D amplitude equations is used, and in the far field the analytic solution of phase equations corresponding to stationary moving PHD is found. The overall mobility tensor is obtained by combining the two contributions. The resulting closed set of algebraic equations for PHD velocity vector contains only three numerical $O(1)$ constants. In Section 4 we compare predictions of the theoretical model with direct numerical integration of amplitude equations. Section 5 contains the results of numerical investigation of interaction of PHDs in optimal hexagonal patterns. Contrary to our expectations, these results are at least in qualitative agreement with oversimplified theory which treats each defect motion in a static field of the other. Section 6 summarizes the results of the paper.

A short account of this work has been published in letter [15].

2. Amplitude equations

The order parameter of the hexagonal pattern is written in the form $a = \epsilon^{1/2} \sum_{j=1}^3 A_j \exp(i\mathbf{k}_j \mathbf{r}) + \text{c.c.}$, where ϵ is a small parameter characterizing the distance above onset, all three $|\mathbf{k}_i| = k_0$, an onset wavenumber of the symmetry-breaking instability, \mathbf{k}_1 points at the x direction (polar angle $\phi = 0$), and $\mathbf{k}_{2,3}$ point at $\phi = \pm 2\pi/3$, respectively. Complex amplitudes A_j are slow functions of $\mathbf{R} = \epsilon^{1/2} \mathbf{r}$ and $T = \epsilon t$. A_j satisfy the following triplet of equations [10]:

$$\partial_T A_j = \mu A_j + A_{j-1}^* A_{j+1}^* - (|A_j|^2 + \gamma |A_{j-1}|^2 + \gamma |A_{j+1}|^2) A_j + (\mathbf{n}_j \cdot \nabla)^2 A_j. \quad (1)$$

Here \mathbf{n}_j is the unit vector oriented along the wavevector of wave j ,

$$\begin{aligned} \mathbf{n}_1 &= (1, 0), & \mathbf{n}_2 &= \left(-\frac{1}{2}, \frac{1}{2}\sqrt{3}\right), \\ \mathbf{n}_3 &= \left(-\frac{1}{2}, -\frac{1}{2}\sqrt{3}\right), \end{aligned} \quad (2)$$

index j is defined modulo 3, the coefficient of quadratic nonlinearity is rescaled to unity, μ is the rescaled supercriticality parameter, γ is the ratio of the coefficient of cubic interaction of rolls of different orientation to the coefficient of cubic self-interaction, and spatial gradients are calculated with respect to slow variable \mathbf{R} . Asterisks denote the complex conjugate. The applicability of these equations to the description of real hexagonal patterns has been discussed earlier [7,10,16].

Since we are interested in non-optimal hexagonal patterns, we will take the complex amplitudes A_j in the form $A_j = B_j \exp(i\mathbf{K}_j \mathbf{R})$, where vectors \mathbf{K}_j are rescaled corrections to the optimal wavevectors \mathbf{k}_j , $\sum_{j=1}^3 \mathbf{K}_j = 0$ as the resonance condition must hold for non-optimal patterns as well. The equations for B_j follow directly from (1),

$$\begin{aligned} \partial_T B_j &= (\mu - K_j^2) B_j + B_{j-1}^* B_{j+1}^* \\ &\quad - (|B_j|^2 + \gamma |B_{j-1}|^2 + \gamma |B_{j+1}|^2) B_j \\ &\quad + (\mathbf{n}_j \cdot \nabla)^2 B_j + 2iK_j (\mathbf{n}_j \cdot \nabla) B_j, \end{aligned} \quad (3)$$

where $K_j = (\mathbf{n}_j \cdot \mathbf{K}_j)$. Eqs. (3) have a family of uniform stationary solutions, B_j^0 , of which only the

equilateral one ($K_j = K$) can be expressed in a simple analytic form,

$$B_1^0 = B_2^0 = B_3^0 = B_0 \\ \equiv \frac{1 + \sqrt{1 + 4(\mu - K^2)(1 + 2\gamma)}}{2(1 + 2\gamma)}. \quad (4)$$

In a general case of different K_j the amplitudes B_j are different, and the solutions are known as rhombic patterns. Stability properties of nonequilateral rhombic patterns were studied recently in Refs. [12,13].

A spontaneously formed hexagonal pattern is usually defect-ridden. Various defects have been described in the literature (see, for example, [3]). Most of them are not stable and either disappear quickly or transform into basic penta–hepta defects. As it was mentioned before, PHD is a bound state in which any two modes have dislocations with opposite winding numbers. It is easy to conclude that this defect is stationary in the optimal hexagonal pattern with all $K_j = 0$. In fact, it follows directly from the variational nature of the model (1) (see [17]). Without loss of generality we will consider a particular form of the penta–hepta defect with positive dislocation in mode 2 and negative dislocation in mode 3. Mode 1 contains no dislocations. A corresponding solution to (1) can be written in the form

$$A_j = F_j(R, \phi) e^{i\theta_j(R, \phi)}, \quad (5)$$

where R and ϕ are polar coordinates, $\oint_C \nabla \theta_1 ds = 0$, $\oint_C \nabla \theta_{2,3} ds = \pm 2\pi$, $F_{1,2}(0, \phi) = 0$, $F_{1-3}(\infty, \phi) = B_0$, and C is a closed contour encircling the origin. This solution cannot be expressed in a closed analytic form. However, in the far field where all the amplitudes approach asymptotic value B_0 , the following remarkable solution for the phase fields θ_j depending only on the polar angle ϕ has been found [16]:

$$\theta_1 = (1 - \cos 2\phi) \frac{1}{6} \sqrt{3}, \\ \theta_2 = \phi - \left[\frac{1}{2} - \cos(2\phi - \frac{2}{3}\pi) \right] \frac{1}{6} \sqrt{3}, \\ \theta_3 = -\phi - \left[\frac{1}{2} - \cos(2\phi + \frac{2}{3}\pi) \right] \frac{1}{6} \sqrt{3}. \quad (6)$$

In order to find the equations of motion for the penta–hepta defect in the non-optimal hexagonal pattern we will employ the calculation method outlined

in [18]. Namely, we assume that PHD moves with a constant velocity V , so the solution of (1) can be written in the form

$$A_j = B_j(\mathbf{R} - V\mathbf{T}) e^{i\mathbf{K}_j \cdot \mathbf{R}}. \quad (7)$$

Transforming into a moving frame $\mathbf{R}' = \mathbf{R} - V\mathbf{T}$ then yields the set of stationary equations for $B_j(\mathbf{R}')$ which coincides with (3) with ∂_T replaced by $-V\nabla B_j$,

$$-V\nabla B_j = (\mu - K_j^2) B_j + B_{j-1}^* B_{j+1}^* \\ - (|B_j|^2 + \gamma |B_{j-1}|^2 + \gamma |B_{j+1}|^2) B_j \\ + (\mathbf{n}_j \cdot \nabla)^2 B_j + 2iK_j (\mathbf{n}_j \cdot \nabla) B_j. \quad (8)$$

To find a relation between V and K_j we project (8) onto its two orthogonal translational modes, $\{\partial_X B_j^*\}$ and $\{\partial_Y B_j^*\}$,

$$I_{xx} V_x + I_{xy} V_y \\ = -i \left\langle \sum_{j=1}^3 K_j \partial_X B_j^* (\mathbf{n}_j \cdot \nabla) B_j - \text{c.c.} \right\rangle, \quad (9)$$

$$I_{xy} V_x + I_{yy} V_y \\ = -i \left\langle \sum_{j=1}^3 K_j \partial_Y B_j^* (\mathbf{n}_j \cdot \nabla) B_j - \text{c.c.} \right\rangle, \quad (10)$$

where

$$I_{xx} = \left\langle \sum_{j=1}^3 |\partial_X B_j|^2 \right\rangle, \\ I_{yy} = \left\langle \sum_{j=1}^3 |\partial_Y B_j|^2 \right\rangle, \\ I_{xy} = I_{yx} = \frac{1}{2} \left\langle \sum_{j=1}^3 \partial_X B_j \partial_Y B_j^* + \text{c.c.} \right\rangle, \quad (11)$$

and $\langle \dots \rangle = \iint \dots dX dY$. All other terms from the r.h.s. of Eq. (8) vanish upon integration under usual boundary conditions at infinity. After simple transformations the resulting equations take the form

$$\hat{\mathbf{I}} \cdot \mathbf{V} \equiv \begin{pmatrix} I_{xx} & I_{xy} \\ I_{yx} & I_{yy} \end{pmatrix} \begin{pmatrix} V_x \\ V_y \end{pmatrix} = \begin{pmatrix} T_1 \\ T_2 \end{pmatrix}, \quad (12)$$

where $\hat{\mathbf{I}}$ is a contravariant mobility tensor,

$$\begin{aligned} T_1 &= -\sqrt{3}\pi[|B_2^0|^2 K_2 + |B_3^0|^2 K_3], \\ T_2 &= \pi[|B_3^0|^2 K_3 - |B_2^0|^2 K_2]. \end{aligned} \quad (13)$$

Here we used the formula

$$\langle \partial_X B_j \partial_Y B_j^* \rangle - \text{c.c.} = 2\pi i \delta_j |B_j^0|^2, \quad (14)$$

where δ_j is a winding number of the dislocation at the particular mode, $\delta_1 = 0$, and $\delta_{2,3} = \pm 1$, respectively.

We will also need an alternative form for the equations of motion (12) written in the coordinate frame (ξ, η) where $\xi = X \cos \psi + Y \sin \psi$ is the coordinate along the defect motion, and $\eta = Y \sin \psi - X \cos \psi$ orthogonal to that (ψ is the angle between the direction of defect motion and X -axis). Projection of (8) onto $\{\partial_\xi B_j^*\}$ and $\{\partial_\eta B_j^*\}$ yields

$$\begin{pmatrix} I_{\xi\xi} & I_{\xi\eta} \\ I_{\eta\xi} & I_{\eta\eta} \end{pmatrix} \begin{pmatrix} V \\ 0 \end{pmatrix} = \begin{pmatrix} \bar{T}_1 \\ \bar{T}_2 \end{pmatrix}, \quad (15)$$

where

$$\begin{aligned} I_{\xi\xi} &= \left\langle \sum_{j=1}^3 |\partial_\xi B_j|^2 \right\rangle, \\ I_{\eta\eta} &= \left\langle \sum_{j=1}^3 |\partial_\eta B_j|^2 \right\rangle, \\ I_{\xi\eta} &= I_{\eta\xi} = \frac{1}{2} \left\langle \sum_{j=1}^3 \partial_\xi B_j \partial_\eta B_j^* + \text{c.c.} \right\rangle, \\ \bar{T}_1 &= 2\pi[|B_2^0|^2 K_2 \sin(\psi - \frac{2}{3}\pi) \\ &\quad - |B_3^0|^2 K_3 \sin(\psi + \frac{2}{3}\pi)], \\ \bar{T}_2 &= 2\pi[|B_2^0|^2 K_2 \cos(\psi - \frac{2}{3}\pi) \\ &\quad - |B_3^0|^2 K_3 \cos(\psi + \frac{2}{3}\pi)]. \end{aligned} \quad (16)$$

3. Mobility tensor of a penta–hepta defect

The first conclusion which can be drawn from (12)–(16) is that indeed PHD is immobile in ideal hexagonal patterns with $K_j = 0$. Magnitude and direction of motion of PHD in non-optimal pattern is determined by the wavevectors of the modes containing singularities and the mobility tensor $\hat{\mathbf{I}}$.

The well-known difficulty in treating equations of motions for topological defects is that integrals en-

tering their mobilities diverge at large distances when stationary solutions are used in the integrands. Indeed, with the static phase approximation solution (5),(6) components of $\hat{\mathbf{I}}$ diverge logarithmically at both small and large R . Evidently, the phase approximation is not valid at small R where stationary solution of full amplitude Eqs. (3) should be employed. The more serious problem arises at large R . Of course, one can introduce an *ad hoc* large-scale cut-off due to finite-size effects, and therefore the mobility will be logarithmically dependent on the size of the box. This may be relevant only for small systems ($VR_{\text{box}} \ll 1$). Another possibility widely considered in the literature for regular dislocations is to use solutions corresponding to moving defects¹. It has been shown that in this case the integrals converge and therefore a finite velocity of dislocations can be found even in the large box limit ($VR_{\text{box}} \gg 1$). In this section, we will calculate the mobility of the moving penta–hepta defect in the spirit of the calculation scheme [17,18], i.e. assuming that all K_j are small, therefore the velocity of PHD is also small, and all $O(K^2)$ corrections in the r.h.s. of (3) can be omitted. For $|V| \ll 1$, the solution describing moving defect differs from the stationary one only at large distances $R \sim V^{-1} \gg 1$, where the phase approximation is well justified. Therefore, the region of integration for the components of the mobility tensor can be split into two parts; in the inner region ($R < R_0$, where $1 \ll R_0 \ll |V|^{-1}$) the stationary PHD solution can be used, and in the outer region ($R > R_0$) the phase approximation can be used to simplify the task of finding the moving PHD solution. So, the mobility tensor can be rewritten in a form

$$\begin{aligned} \hat{\mathbf{I}} &= \begin{pmatrix} I_{xx}^{(1)} + I_{xx}^{(2)} & I_{xy}^{(1)} + I_{xy}^{(2)} \\ I_{yx}^{(1)} + I_{yx}^{(2)} & I_{yy}^{(1)} + I_{yy}^{(2)} \end{pmatrix} \\ &= \begin{pmatrix} I_{\xi\xi}^{(1)} + I_{\xi\xi}^{(2)} & I_{\xi\eta}^{(1)} + I_{\xi\eta}^{(2)} \\ I_{\eta\xi}^{(1)} + I_{\eta\xi}^{(2)} & I_{\eta\eta}^{(1)} + I_{\eta\eta}^{(2)} \end{pmatrix}, \end{aligned} \quad (17)$$

¹ Strictly speaking, the asymptotic matching procedure outlined in [19] is a better method to avoid divergencies in such problems. Unfortunately, in the present context, it does not seem feasible to implement. Note, however, that tedious asymptotic analysis of vortex motion in a real Ginzburg–Landau equation [19] produced results which agreed quantitatively with the simpler, albeit mathematically less rigorous approach [18] employed here.

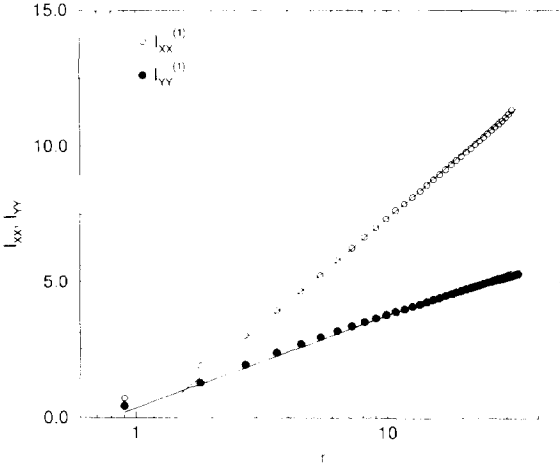


Fig. 1. Near field components of mobility tensor $I_{xx}^{(1)}$ and $I_{yy}^{(1)}$ as function of R_0 . Results of direct simulations of amplitude equations (1) with $\mu = 1$, $\gamma = 2$ have been used. Logarithmic dependence on R_0 is clearly seen.

We expect that at $R \approx R_0$ stationary phase approximation solution (5),(6) should be applicable, and therefore

$$\begin{aligned} I_{xx}^{(1,2)} &= a_1 B_0^2 \ln(C_{xx}^{(1,2)} R_0^{\pm 1}), \\ I_{yy}^{(1,2)} &= a_2 B_0^2 \ln(C_{yy}^{(1,2)} R_0^{\pm 1}), \\ I_{xy}^{(1,2)} &= B_0^2 C_{xy}^{(1,2)}, \end{aligned} \quad (18)$$

where from (6), $a_1 = 7\pi/2$, $a_2 = 3\pi/2$. $C_{ln}^{(1)}$ can be only functions of parameters μ and γ , but $C_{ln}^{(2)}$ can also depend on V itself (subscripts l and n stand for either x or y). In virtue of symmetry of the stationary solution with respect to X -axis, $C_{xy}^{(1)} = 0$, and $I_{xy}^{(2)}$ is independent of R_0 . After adding two parts of the integrals together radius R_0 should drop out.

Let us first consider the inner region $R < R_0$. Unfortunately, even the simplified problem of finding the static PHD solution of (3) near the core cannot be reduced to ODE. All we can do is to find the stationary solution numerically by integrating 2D amplitude equations (3) for any given μ and γ (for a detailed discussion of numerical simulations of the amplitude equations see Section 4). In Fig. 4 of Ref. [7] the structure of the penta-hepta defect is shown for a particular set of parameters $\mu = 1$, $\gamma = 2$. In Fig. 1 components $I_{xx}^{(1)}$ and $I_{yy}^{(1)}$ are shown as functions of R_0 for the same values μ and γ . They indeed behave logarithmically

as expected with $a_1 = 10.78$, $a_2 = 4.17$ which is in good agreement with exact prefactors following from the phase approximation. Constants $C_{ln}^{(1)}$ can be extracted from these dependencies. For the chosen parameters, $C_{xx}^{(1)} = 0.86$, $C_{yy}^{(1)} = 1.28$. Constant $C_{xy}^{(1)}$ was found to be < 0.01 .

Now we calculate the second part of the mobility tensor using the phase approximation, or by assuming that the amplitudes of all three waves are constants. The components of the mobility tensor will take the form

$$\begin{aligned} I_{xx}^{(2)} &= \left\langle \sum_{j=1}^3 |B_j^0|^2 (\partial_x \theta_j)^2 \right\rangle, \\ I_{yy}^{(2)} &= \left\langle \sum_{j=1}^3 |B_j^0|^2 (\partial_y \theta_j)^2 \right\rangle, \\ I_{xy}^{(2)} &= \left\langle \sum_{j=1}^3 |B_j^0|^2 \partial_x \theta \partial_y \theta_j \right\rangle, \end{aligned} \quad (19)$$

where angular brackets now denote the integration over the $R > R_0$ region. The simple-minded approach consists in using the static solution (6) in these expressions. We already mentioned before that in this case the integrals diverge logarithmically, so the finite answer can be obtained only for the finite size box, and the consistency of calculation can be checked *a posteriori* by verifying condition $VR_{\text{box}} \ll 1$. Direct calculation using (6) gives

$$\begin{aligned} I_{xx}^{(2)} &= \frac{7}{2} \pi B_0^2 \ln(R_{\text{box}}/R_0), \\ I_{yy}^{(2)} &= \frac{3}{2} \pi B_0^2 \ln(R_{\text{box}}/R_0), \\ I_{xy}^{(2)} &= 0, \end{aligned} \quad (20)$$

so summation of (18) and (20) produces the same result (18) with R_0 replaced by R_{box} . The condition of validity of this approximation is therefore $KR_{\text{box}} [\ln R_{\text{box}}]^{-1} \ll 1$, where $K = O(K_j)$.

In the more natural opposite limit we have to correct the solution by finding the phase field of a moving defect. To this end we will use the stationary phase equations in the moving frame (cf. [7,16]),

$$-(V \cdot \nabla) \theta_j = -B_0 \sin \Phi + (\mathbf{n}_j \cdot \nabla)^2 \theta_j, \quad (21)$$

where $\Phi = \theta_1 + \theta_2 + \theta_3$. To account for the phase winding around PHD, we have to impose circulation conditions $\theta_1(R, 2\pi) - \theta_1(R, 0) = 0$, $\theta_2(R, 2\pi) - \theta_2(R, 0) = 2\pi$, $\theta_3(R, 2\pi) - \theta_3(R, 0) = -2\pi$. Following [16], we can exclude $\sin \Phi$ from (21) and replace θ_1 by $-(\theta_2 + \theta_3)$ since the total phase Φ converges to zero in the far field. The remaining equations can be conveniently written for the variables $\theta^\pm = \theta_2 \pm \theta_3$,

$$\begin{aligned} \mathbf{V} \cdot \nabla \theta^+ + \frac{3}{4} \theta_{XX}^+ + \frac{1}{4} \theta_{YY}^+ &= \frac{1}{6} \sqrt{3} \theta_{XY}^-, \\ \mathbf{V} \cdot \nabla \theta^- + \frac{1}{4} \theta_{XX}^- + \frac{3}{4} \theta_{YY}^- &= \frac{1}{2} \sqrt{3} \theta_{XY}^+. \end{aligned} \quad (22)$$

Subscripts at the phase variables θ^\pm here and below denote partial differentiation. In order to preserve the circulation conditions for θ^+ and θ^- ,

$$\begin{aligned} \theta^+(R, 2\pi) - \theta^+(R, 0) &= 0, \\ \theta^+(R, 2\pi) - \theta^+(R, 0) &= 4\pi, \end{aligned} \quad (23)$$

we should introduce appropriate source terms on the r.h.s. of (22). Without loss of generality, we place a branch cut along the direction of the defect motion $\xi > 0$, $\eta = 0$. We also rescale space variables by the modulus of the defect velocity V . As a result we obtain

$$\begin{aligned} \theta_\xi^+ + \frac{3}{4} \theta_{XX}^+ + \frac{1}{4} \theta_{YY}^+ &= \frac{1}{6} \sqrt{3} \theta_{XY}^- \\ &- \frac{2}{3} \sqrt{3} \pi \sin 2\psi \delta'(\xi) H(\eta) \\ &+ \frac{1}{6} \sqrt{3} \pi (4 \sin^2 \psi - 1) \delta(\xi) \delta(\eta), \\ \theta_\xi^- + \frac{1}{4} \theta_{XX}^- + \frac{3}{4} \theta_{YY}^- &= \frac{1}{2} \sqrt{3} \theta_{XY}^+ \\ &+ \pi (2 \sin^2 \psi + 1) \delta'(Y) H(x) \\ &+ \pi \sin 2\psi \delta(\xi) \delta(\eta) + 4\pi \delta(\xi) H(\eta). \end{aligned} \quad (24)$$

Here $\delta(x)$ is a Dirac delta function, and $H(x)$ is a Heaviside function. Solution of (24) can be found in Fourier space (we present here the Fourier images of derivatives $\theta_{\xi,\eta}^\pm$),

$$\begin{aligned} \tilde{\theta}_\xi^+ &= -\frac{2\pi i}{\sqrt{3}} k_\xi (k_y^2 - k_x^2 + 4ik_x \cos \psi - \frac{4}{3} ik_y \sin \psi) Q, \\ \tilde{\theta}_\eta^+ &= -\frac{2\pi i}{\sqrt{3}} k_\eta (k_y^2 - k_x^2 + 4ik_x \cos \psi - \frac{4}{3} ik_y \sin \psi) Q, \\ \tilde{\theta}_\xi^- &= -\frac{4}{3} \pi i [(2k_y k_x^2 + k_y^3) \sin \psi + k_x^3 \cos \psi \\ &- \frac{4}{3} (-2k_\xi k_\eta - k_\xi k_\eta \cos 2\psi - k_\xi^2 \sin 2\psi)] Q, \end{aligned}$$

$$\begin{aligned} \tilde{\theta}_\eta^- &= -\frac{4}{3} \pi i [(2k_y k_x^2 + k_y^3) \cos \psi + k_x^3 \sin \psi \\ &- \frac{4}{3} (4k_\xi^2 + 2k_\eta^2 - 4ik_\xi - k_\xi k_\eta \sin 2\psi \\ &- k_\eta^2 \cos 2\psi)] Q, \end{aligned} \quad (25)$$

where

$$Q = [(k^2 + 4ik_\xi)(k^2 + \frac{4}{3} ik_\eta)]^{-1}. \quad (26)$$

Solutions (25) can be readily inverted back to the real space by making use of two useful Fourier integrals,

$$\begin{aligned} \int 2\pi i k_\xi Q e^{ikr} d^2k &= F(\xi, \eta) \\ &\equiv \frac{3}{8} [K_0(\frac{2}{3}R) e^{-2\xi/3} - K_0(2R) e^{-2\xi}], \\ \int 2\pi k_\eta^2 Q e^{ikr} d^2k &= G(\xi, \eta) \\ &\equiv \frac{1}{2} [3K_0(2R) e^{-2\xi} - K_0(\frac{2}{3}R) e^{-2\xi/3}] + \partial_\xi F. \end{aligned} \quad (27)$$

Here K_0 is a modified Bessel function of zeroth order. The resulting expressions for phase derivatives read

$$\begin{aligned} \theta_\xi^+ &= \frac{1}{\sqrt{3}} [\frac{4}{3} F_\xi + \sin 2\psi (2F_{\xi\eta} - \frac{8}{3} F_\eta) \\ &+ \cos 2\psi (\frac{8}{3} F_\xi + F_{\eta\eta} - F_{\xi\xi})], \\ \theta_\eta^+ &= \frac{1}{\sqrt{3}} [\frac{4}{3} F_\eta + \sin 2\psi (2F_{\eta\eta} - \frac{8}{3} G) \\ &+ \cos 2\psi (\frac{8}{3} F_\eta + G_\eta - F_{\xi\eta})], \\ \theta_\xi^- &= 2F_{\xi\eta} + 2G_\eta - \frac{16}{3} F_\eta \\ &+ \sin 2\psi (F_{\xi\xi} - F_{\eta\eta} - \frac{8}{3} F_\xi) \\ &+ \cos 2\psi (2F_{\xi\eta} - \frac{8}{3} F_\eta), \\ \theta_\eta^- &= -2F_{\xi\xi} + 2F_{\eta\eta} + \frac{16}{3} (2F_\xi + G - 2F) \\ &+ \sin 2\psi (F_{\xi\eta} - G_\eta - \frac{8}{3} F_\eta) \\ &+ \cos 2\psi (2F_{\eta\eta} - \frac{8}{3} G), \end{aligned} \quad (28)$$

(subscripts ξ and η at F, G denote partial differentiation). Analysis of expressions (28) shows that, as in case of moving dislocations in roll patterns [17,18], phase distortions decay exponentially in front of the defect (at $\xi \rightarrow \infty$) and decay algebraically behind the defect (at $\xi \rightarrow -\infty$). Distributions of $\partial_\eta \theta_{1-3}$ for $V = 0$ and $V = 0.1$ are shown in Fig. 2.

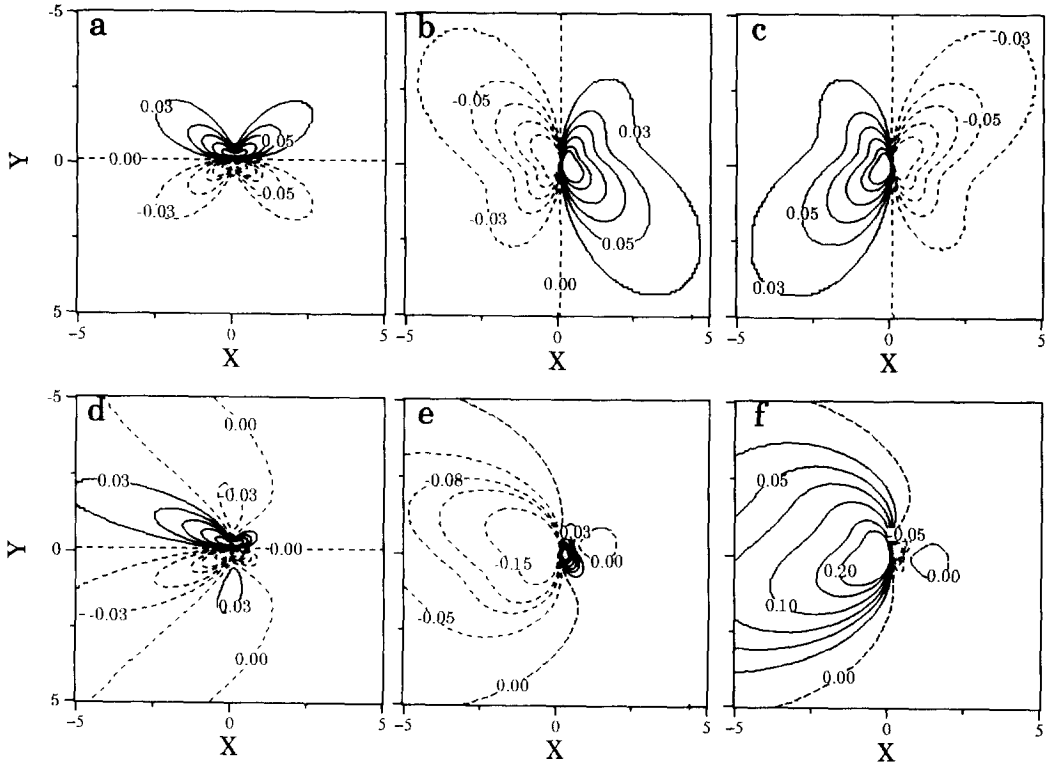


Fig. 2. Isolines of $\partial_\gamma \theta_{1,2,3}$ for immobile PHD (a)–(c), and a PHD moving along X -direction (d)–(f).

Using expressions (28) it is convenient to compute the longitudinal $I_{\xi\xi}^{(2)}$ and cross $I_{\xi\eta}^{(2)}$ terms in (17) (we do not need the component of the mobility $I_{\eta\eta}$ orthogonal to the direction of motion):

$$\begin{aligned}
 I_{\xi\xi}^{(2)} &\equiv B_0^2 \langle (\theta_\xi^+)^2 + \frac{1}{4}(\theta_\xi^- + \theta_\xi^+)^2 + \frac{1}{4}(\theta_\xi^- - \theta_\xi^+)^2 \rangle, \\
 I_{\xi\eta}^{(2)} &\equiv B_0^2 \langle \theta_\xi^+ \theta_\eta^+ + \frac{1}{4}(\theta_\xi^- + \theta_\xi^+)(\theta_\eta^- + \theta_\eta^+) \\
 &\quad + \frac{1}{4}(\theta_\xi^- - \theta_\xi^+)(\theta_\eta^- - \theta_\eta^+) \rangle
 \end{aligned} \quad (29)$$

(here $\langle \dots \rangle$ means integration outside the circle of radius VR_0). In virtue of symmetry of functions F and G with respect to η -axis many terms in resulting expressions vanish upon integration. The final expressions are relatively simple (tedious intermediate algebra was performed using the MAPLE V package),

$$\begin{aligned}
 I_{\xi\xi}^{(2)} &= B_0^2 (g_1 + g_2 \cos 2\psi), \\
 I_{\xi\eta}^{(2)} &= B_0^2 g_3 \sin 2\psi,
 \end{aligned} \quad (30)$$

where

$$\begin{aligned}
 g_1 &= \langle 2G_\eta^2 + \frac{1}{2}G_{\xi\xi}^2 - F_{\xi\xi}F_{\eta\eta} + \frac{160}{9}F_\eta^2 + 4F_{\xi\eta} \\
 &\quad - \frac{32}{3}F_\eta G_\eta + \frac{8}{3}F_\xi F_{\eta\eta} + \frac{1}{2}F_{\eta\eta}^2 + 4F_{\xi\eta}^2 + \frac{40}{9}F_\xi^2 \rangle, \\
 g_2 &= \langle \frac{128}{9}F_\eta^2 + \frac{4}{3}F_\xi F_{\eta\eta} + 4F_{\xi\eta}^2 - \frac{16}{3}F_\eta G_\eta \\
 &\quad + 4F_{\xi\eta} G_\eta + \frac{32}{9}F_\xi^2 \rangle, \\
 g_3 &= \langle \frac{4}{3}(-F_\xi F_{\eta\eta} - 4F_{\xi\xi}F + 4F_\eta^2 + 4F_{\eta\eta}F \\
 &\quad - 2F_{\eta\eta}G + 2F_{\xi\xi}G) - \frac{80}{9}F_\xi G - \frac{128}{9}F_\xi^2 + F_{\xi\eta}^2 \\
 &\quad - 4F_{\xi\eta}F_\eta - G_\eta^2 + F_{\eta\eta}^2 - F_{\xi\xi}^2 \rangle.
 \end{aligned} \quad (31)$$

Integrals g_{1-3} can be reduced to one-dimensional ones by analytic integration over the polar angle from 0 to 2π . The resulting one-dimensional integrals over the radius should be computed from VR_0 to ∞ (we return now to original space variables). Numerical integration yields $g_l = -c_l \ln(s_l VR_0)$, $l = 1, 2, 3$, with $c_1 = 7.90$, $c_2 = c_3 = 3.15$, $s_1 = s_3 = 0.78$, $s_2 = 0.73$. The above quite cumbersome calculation can be verified using simple relations between tensor components

$$I_{\xi\xi}^{(2)} = I_{xx} \cos^2 \psi + I_{yy} \sin^2 \psi + I_{xy} \sin 2\psi,$$

$$I_{\xi\eta}^{(2)} = \frac{1}{2}(I_{yy} - I_{xx}) \sin 2\psi + I_{xy} \cos 2\psi, \quad (32)$$

and (18). From comparing (30) with (32) it is easy to conclude that conditions

$$\frac{1}{2}(a_1 - a_2) = c_2 = c_3, \quad \frac{1}{2}(a_1 + a_2) = c_1 \quad (33)$$

should hold, which indeed is true within the accuracy of numerical integration.

It remains to combine (18) with (30) to obtain the expressions for mobility tensor components for PHD. Making use of (32) again, we get

$$\begin{aligned} I_{\xi\xi} &= B_0^2 \frac{1}{4} \pi (7 \ln C_{xx}^{(1)} \cos^2 \psi + 3 \ln C_{yy}^{(1)} \sin^2 \psi \\ &\quad - 5 \ln(s_1 V) - 2 \ln(s_2 V) \cos 2\psi) \\ &= -B_0^2 \left[\frac{5}{2} \pi \ln(w_1 V) + \pi \cos 2\psi \ln(w_2 V) \right] \\ I_{\xi\eta} &= B_0^2 \frac{1}{4} \pi [3 \ln C_{yy}^{(1)} - 7 \ln C_{xx}^{(1)} + 4 \ln(s_3 V)] \sin 2\psi \\ &= B_0^2 \pi \sin 2\psi \ln(w_3 V), \end{aligned} \quad (34)$$

where $w_1 = 1.24$, $w_2 = 1.14$, $w_3 = 2.00$.

Now we can substitute (16) and (34) into (15). Since we already assumed all three K_j small, without further loss of accuracy we can take in (16) all three $|B_j| = B_0$ after which it is cancelled. In this way we obtain a set of two nonlinear algebraic equations for V and ψ ,

$$\begin{aligned} \frac{5}{2} V \ln(w_1 V) + V \ln(w_2 V) \cos 2\psi \\ = -2K_2 \sin(\psi - \frac{2}{3}\pi) + 2K_3 \sin(\psi + \frac{2}{3}\pi), \end{aligned} \quad (35)$$

$$\begin{aligned} V \ln(w_3 V) \sin 2\psi = 2K_2 \cos(\psi - \frac{2}{3}\pi) \\ - 2K_3 \cos(\psi + \frac{2}{3}\pi) \end{aligned} \quad (36)$$

In these equations there are only three $O(1)$ constants which (for small K_j) are functions of parameters μ , γ only². For each set of these parameters together with K_{1-3} a unique velocity vector \mathbf{V} is found. In the next section we will compare predictions of this asymptotic theory with numerical simulations of amplitude equations.

²More precisely, constants s_{1-3} are universal and only $C_{xx}^{(1)}$, $C_{yy}^{(1)}$ which come from the core contribution, depend on ν and γ .

Eqs. (15) have been written for a particular penta-hepta defect with positive dislocation in the second mode, negative dislocation in the third mode and no dislocation in the first mode. For brevity, it can be labeled as $(0, 1, -1)$. As we discussed earlier, due to synchronization of waves a sum of three indices must be always zero. In general, there exist only three topologically different penta-hepta defects, $(0, 1, -1)$, $(1, 0, -1)$, $(1, -1, 0)$, and their mirror images (conjugate defects) $(0, -1, 1)$, $(-1, 0, 1)$, $(-1, 1, 0)$. The equations of motion for two other penta-hepta defects, $(1, 0, -1)$, $(1, -1, 0)$ can be obtained from Eqs. (36) by cyclic relabeling of $K_{1,2,3}$ and replacing ψ by $\psi \pm \frac{2}{3}\pi$. For conjugate PHDs, the mobility tensor remains the same, but the r.h.s. of equations of motion change sign. Obviously, for conjugate defects, $V^* = V$ and $\psi^* = \psi + \pi$.

4. Numerical simulations of amplitude equations

Numerical simulations of the set of amplitude equations (3) were performed using a split-step method. Linear parts were integrated using FFT, and nonlinear parts were calculated using the Euler integrator. Typically we used 256×256 spatial harmonics with periodic boundary conditions; physical system size was 100×100 or smaller, and the time step was chosen 0.1. In all examples described below $\mu = 1$, $\gamma = 2$.

As initial conditions we usually take $(0, 1, -1)$ defect placed in the middle of the integration domain. To diminish an effect of periodic boundary conditions we introduce a circular ramp at $R > 0.4l$. The location of the core of PHD was determined by finding minima of $|B_2|$, $|B_3|$, and the velocity vector was calculated from the linear regression of time variations of X and Y coordinates of core.

At first we took $K_1 = K_2 = 0$ and varied only the wavenumber correction K_3 . In Fig. 3 the magnitude and angle of the velocity vector found from (15) are plotted together with the results of direct numerical simulations. From the theoretic model we expect only weak logarithmic dependence of ψ on K_3 , and indeed, simulations demonstrate that the direction of motion stays practically unchanged, except for the jump of π

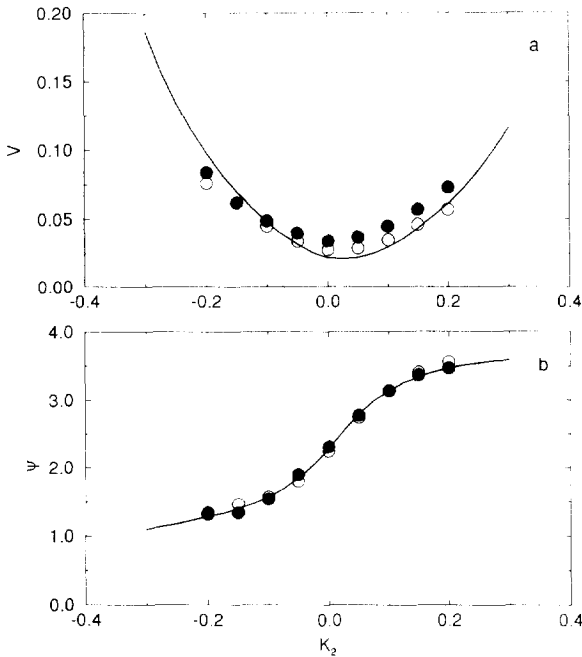


Fig. 3. Velocity vector of a PHD $(0, 1, -1)$ as a function of wavenumber correction K_2 at $K_1 = 0$, $K_3 = 0$; (a) magnitude, (b) angle with respect to X -axis, parameters $\mu = 1$, $\gamma = 2$. Solid lines – theory, Eqs. (36), open circles – numerical simulations of (3) with system size $L = 40$, solid circles – same for $L = 100$.

when K_3 changes sign. The magnitude of the velocity scales almost linearly with K_3 . Quantitative comparison indicates that both the direction of motion and the magnitude of velocity are in a good agreement with the theoretical predictions. We checked the importance of finite-size effects by computing velocity for a smaller system size $L = 40$. The results remained practically unchanged.

Now we take $K_1 = 0$ and both K_2 and K_3 non-zero. In Fig. 4 the magnitude and angle of the velocity vector are shown as functions of K_2 for a fixed value of K_3 . Now, the direction of PHD motion strongly depends on the combination of the wavenumber corrections. Again, as in the previous case, the velocity vector is predicted quite well by the asymptotic theory. In a particular case $K_2 = K_3$ it is easy to see that $\psi = 0$ satisfies system (15) exactly, so the PHD in this case moves along X -axis, i.e. parallel to the wavevector of the first (non-singular) mode.

At last, we checked the case when all three K_j are

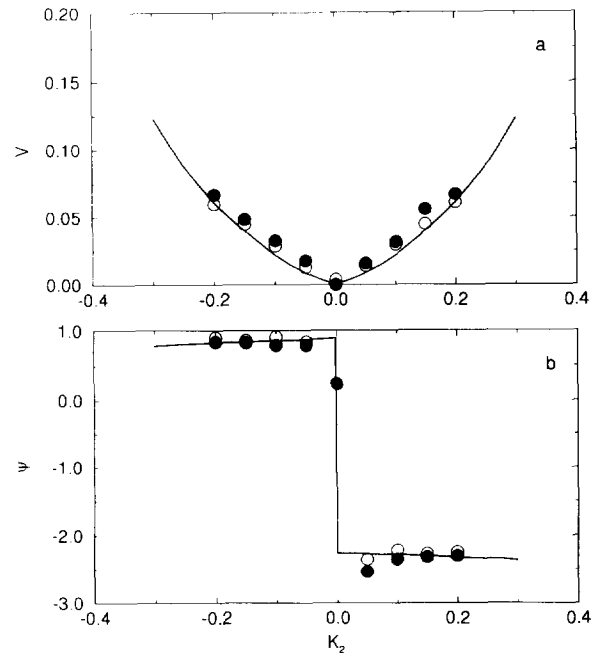


Fig. 4. Same as in Fig. 3 with $K_3 = 0.1$.

non-zero and varied the value of K_1 . Eqs. (15) predict that for small K_j there should be no effect of K_1 on the dynamics of PHD. Only at large K_j when the amplitudes deviate significantly from the value B_0 (this effect was neglected in Section 3 to simplify the mobility computation) the penta–hepta defect starts to “feel” K_1 . Numerical simulations also confirm this prediction (see Fig. 5). Notice that even if all three wavevectors are equal (but non-optimal), PHD still moves along the X -axis.

5. Interaction of penta–hepta defects

One is tempted to apply the equations of motion (36) directly to the interaction of two PHDs. Indeed, when two PHDs are far enough, they interact entirely through the phase perturbations. Each defect distorts the phase field and therefore creates a slightly non-optimal hexagonal pattern at the location of another defect. This simple-minded procedure can be justified if one of two defects is pinned and therefore its phase field is the one of static PHD (6). Such pinning can occur due to a local inhomogeneity in the system,

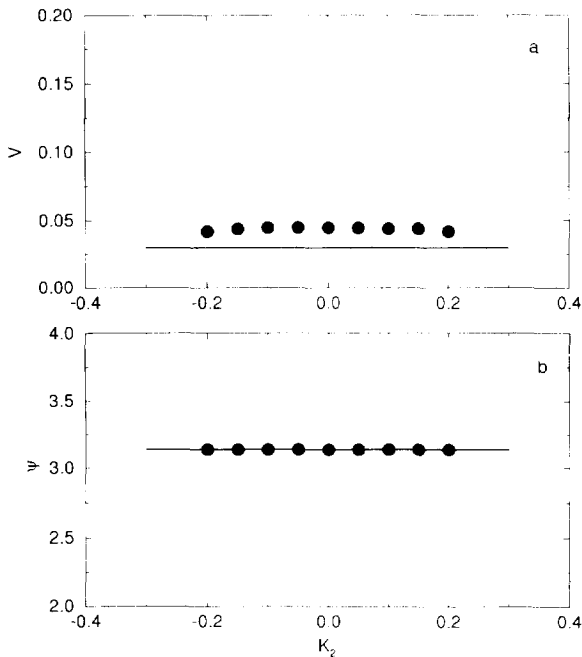


Fig. 5. Velocity vector of a PHD (0,1,-1) as a function of wavenumber correction K_1 at $K_2 = K_3 = 0.1$. The velocity is nearly independent of K_1 .

or may be achieved, for example, by applying active localized control, as described in Ref. [20]. In this case the velocity vector of the “free” PHD is described by Eqs. (36) with wavenumbers K_j in (36) replaced by $\mathbf{n}_j \cdot \nabla \theta_j^{(0)}$ respectively, where $\theta_j^{(0)}$ is the static phase field (6) of the pinned defect. The more realistic case of two free defects is usually much harder, since the phase field of each defect is neither static (6), nor stationary moving (28). Indeed, if we assume that the field is static, and estimate the convergence velocity for a distance R , we obtain $VR \simeq 2$ which clearly is inconsistent with this assumption. Strictly speaking, the phase field “remembers” the whole previous path of the defects.

In this section we present only the results of numerical simulations of interacting penta-hepta defects. To separate the interaction from climbing due to an ambient strain, we now consider an optimal hexagonal pattern (all $K_j = 0$). Trajectories of defects vary significantly with types of interacting defects and their initial positions. In Figs. 6a–d several families of PHD trajectories are shown. The result of interaction (at-

traction or repulsion) of two PHDs, $(\delta_1^1, \delta_2^1, \delta_3^1)$ and $(\delta_1^2, \delta_2^2, \delta_3^2)$, depends on the number

$$N = \sum_{j=1}^3 \delta_j^1 \delta_j^2. \tag{37}$$

Clearly, this number can only take values of $-2, -1, 1,$ and 2 . If $N < 0$ defects attract each other, and in all other cases they repel each other. Fig. 6a illustrates the attraction of two conjugate defects, $(0, 1, -1)$ and $(0, -1, 1)$ (in this case $N = -2$ and defects are attracted). After collision pairs of dislocations at modes 2 and 3 annihilate, and thus perfect hexagonal pattern establishes. Two PHDs of the same type, $(0, 1, -1)$ (here $N = 2$), as expected repel each other (Fig. 6b). More interesting is the case of two different PHDs, say, $(0, 1, -1)$ and $(-1, 0, 1)$, as shown in Fig. 6c. In this case $N = -1$, and defects are attracted again, however complete annihilation does not occur. Instead, conjugate dislocations at mode 3 annihilate, and remaining dislocations at modes 1 (from the first PHD) and 2 (from the second PHD) immediately form a new penta-hepta defect, $(-1, 1, 0)$. As this defect is alone, and the ambient strain is absent, the defect stays put. Fig. 6d shows the trajectories of $(0, 1, -1)$ and $(-1, 0, 1)$ PHDs ($N = 1$). In this case defects are repelled.

In Fig. 7 the distance between two cores is shown as a function of time for interacting $(0, 1, -1)$ and $(0, -1, 1)$ defects. The rate of convergence varies with initial positions of defects. Attraction is strongest for defects aligned along Y -axis, and weakest for defects aligned along the X -axis. Fig. 7a plots the data in the linear coordinates, while Fig. 7b presents the same data in the logarithmic coordinates. Rather unexpectedly, one can see that over large time intervals the data is consistent with $R \propto T^{1/2}$ law, which in turn suggests $V \propto R^{-1}$ scaling. Up to logarithmic corrections this scaling is what one could expect in the static approximation discussed above. We are unable to explain why this seemingly invalid approximation works reasonably well in this case. Furthermore, the same scaling is observed for other PHD configurations as well.

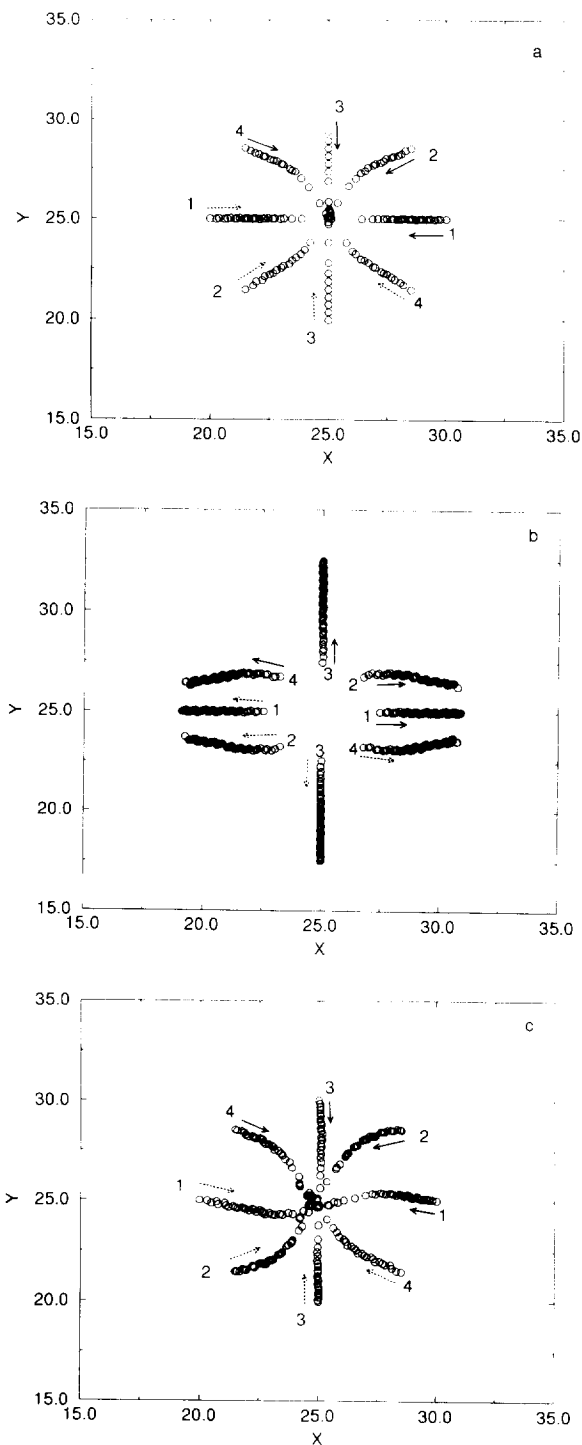


Fig. 6.

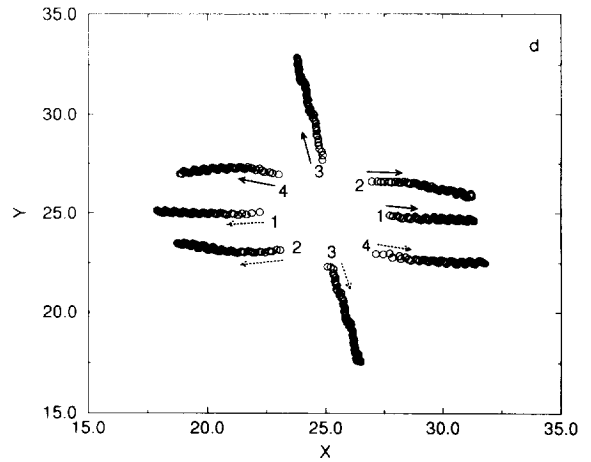


Fig. 6. Trajectories of interacting penta-hepta defects. Open circles indicate positions of the defect cores with time interval $\Delta T = 2.5$. Arrows point toward directions of motion; (a) $(0, 1, -1)$ (solid arrow) and $(0, -1, 1)$ (dotted arrows); (b) $(0, 1, -1)$ (solid arrows) and $(0, 1, -1)$ (dotted arrow); (c) $(0, 1, -1)$ (solid arrow) and $(-1, 0, 1)$ (dotted arrow); (d) $(0, 1, -1)$ (solid arrow) and $(1, 0, -1)$ (dotted arrow). For each case, four sets of initial conditions are taken (they are labeled 1–4 in the figures). In the cases (a),(c) penta-hepta defects attract each other, and in (b),(d) they are repelled.

6. Conclusions

In this paper we investigated the motion of penta-hepta defects in slightly non-optimal hexagonal patterns. The penta-hepta defect represents a bound state of two opposite-signed dislocations on two (of total three) different wave modes. Thus, the penta-hepta defect is a composite anisotropic and even in the phase approximation no scale transformation can reduce the problem to one dimension as in the familiar cases of a Ginzburg–Landau equation [18,19] or a Newell–Whitehead–Segel equation [17,21]. We adopted a potential model of three equations for complex amplitudes of resonantly coupled triplet of modes (1).

Similarly to the well-studied case of dislocation motion in roll patterns, PHD is stationary only in the perfect pattern with wavenumbers of all three modes equal to the onset value (in hexagonal patterns it does not correspond to the boundary of zig-zag instability). In non-optimal hexagonal patterns PHD is driven by the superposition of two Peach–Köhler forces, corresponding to two singular modes. Unlike the well-

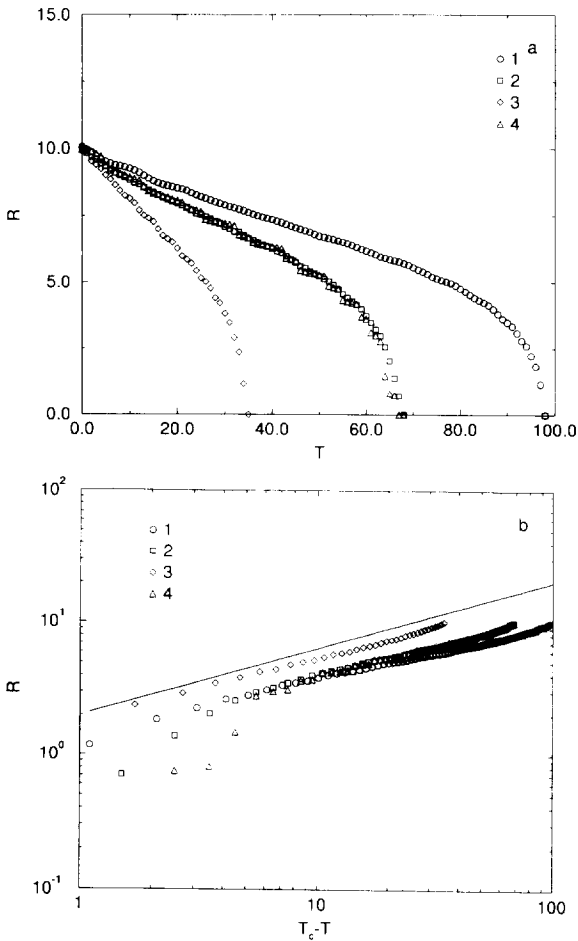


Fig. 7. Distances between interacting penta-hepta defects $(0, 1, -1)$ and $(0, -1, 1)$ versus time; (a) linear coordinates, (b) log-log coordinates. Straight line shows $R \propto T^{1/2}$ law. Labels 1–4 correspond to different initial positions of the defects, as shown in Fig. 6a.

studied case of dislocation motion in roll patterns, the direction of motion cannot be readily determined from symmetry considerations and must be found together with the velocity magnitude from governing equations. Theoretical analysis and numerical simulations were performed in order to find the velocity vector of PHD as a function of wavevector corrections. The main problem was to compute the mobility tensor of penta-hepta defect. In the core region we used a numerical solution of stationary amplitude equations, while in the far field an analytic solution of phase equations has been found. The facilitating factor is that since amplitude equations in the lowest order do not

contain high derivatives (see Refs. [7,16] for discussion), the phase approximation yields linear equations for the phase in the far field. Finally, matching the numerical 2D solution for the PHD core with the analytic solution for the phase in the far field allowed us to arrive at closed expressions for the mobility tensor and obtain the algebraic equations for velocity magnitude and direction. These equations contain only three $O(1)$ numerical constants. For any given combination of wavevector corrections these equations give a unique velocity vector for PHD. Comparison of the theoretical predictions with results of numerical simulations of (3) showed good agreement in both the direction of PHD drift and the magnitude of velocity.

We also studied pair interaction of penta-hepta defects in unstrained hexagonal patterns. PHDs attract or repel each other depending on the parameter N introduced in Section 4. Due to the anisotropic structure, PHDs do not move along the line connecting their cores, and so the trajectories of interacting defects may be rather complicated. Furthermore, when two attracting PHDs collide, they do not necessarily annihilate, but may give birth to another PHD with a different topological structure.

Clearly, Eqs. (1) represent only a simplest possible model for hexagonal pattern formation. More realistic models derived from first principles (see, for example, [14]) usually include non-variational terms. This makes the dynamics of penta-hepta defects yet more interesting. Nevertheless, we expect that major features of PHD dynamics described in this paper will remain unchanged, at least on a qualitative level. We believe that detailed experiments with thermoconvection or parametric ripples similar to ones which have been performed for dislocations in roll patterns [22] could test predictions of our theory.

Acknowledgements

The author is grateful to I. Aranson, H. Levine, and M.I. Rabinovich for useful discussions. This work was supported by the U.S. Department of Energy under contract DE-FG03-95ER14516 and by the Office of Naval Research under contract N00014-D-0142 DO#15.

References

- [1] M. Cross and P. Hohenberg, Pattern formation out of equilibrium, *Rev. Mod. Phys.* 65 (1993) 851.
- [2] E. Bodenschatz, J.R. DeBruyn, G. Ahlers and D.S. Cannell, Transition between patterns in thermal convection, *Phys. Rev. Lett.* 67 (1991) 3078.
- [3] J. Pantaloni and P. Cerisier, Structure defects in Bénard–Marangoni convection, in: *Cellular Structures in Instabilities*, J.E. Weisfreid and S. Zaleski, eds. (Springer, Berlin, 1984).
- [4] W.J. Firth, Hexagon patterns and related phenomena in nonlinear optics, in: *SPIE Proceedings 2039, Chaos in Optics* (1993) 290.
- [5] Q. Ouyang and H.L. Swinney, Transition from a uniform state to hexagonal and striped Turing patterns, *Nature* 352 61 (1991).
- [6] S. Ciliberto, P. Couillet, J. Lega, E. Pampaloni and C. Perez-Garcia, Defects in roll-hexagon competition, *Phys. Rev. Lett.* 65 (1990) 2370.
- [7] M.I. Rabinovich and L.S. Tsimring, Dynamics of dislocations in hexagonal patterns, *Phys. Rev. E* 49 (1993) R35.
- [8] G. Ahlers, private communication.
- [9] B.A. Malomed and M.I. Tribelsky, Stability of stationary periodic structures for weakly supercritical convection and in related problems, *Sov. Phys. JETP* 65 (1987) 305.
- [10] M.M. Sushchik, L.S. Tsimring, The Eckhaus instability in hexagonal patterns, *Physica D* 74 (1994) 90.
- [11] J. Lauzeral, S. Metens and D. Walgraef, On the phase dynamics of hexagonal patterns, *Europhys. Lett.* 24 (1993) 707.
- [12] Q. Ouyang and G.H. Gunaratne and H.L. Swinney, Rhombic patterns: broken hexagonal symmetry, *Chaos* 3 (1993) 707.
- [13] B.A. Malomed, A.A. Nepomnyashchy and A.E. Nuz, Nonequilateral hexagonal pattern, *Physica D* 70 (1994) 357.
- [14] E.A. Kuznetsov, A.A. Nepomnyashchy and L.M. Pismen, The new amplitude equation for Boussinesq convection and nonequilibrium hexagonal patterns, preprint, Technion (1994).
- [15] L.S. Tsimring, Penta-hepta defect motion in hexagonal patterns, *Phys. Rev. Lett.* 74 (1995) 4201.
- [16] L.M. Pismen and A.A. Nepomnyashchy, Structure of dislocations in the hexagonal pattern, *Europhys. Lett.* 24 (1993) 461.
- [17] E.D. Siggia and A. Zippelius, Dynamics of defects in Rayleigh–Bénard convection, *Phys. Rev. A* 24 (1981) 1036; Y. Pomeau, P. Manneville and S. Zaleski, Dislocation motion in cellular structures, *Phys. Rev. A* 27 (1983) 2710; G. Tesauero and M.C. Cross, Climbing of dislocations in nonequilibrium patterns, *Phys. Rev. A* 34 (1986) 1363.
- [18] E. Bodenschatz, W. Pesch and L. Kramer, Structure and dynamics of dislocations in anisotropic pattern-forming systems, *Physica D* 32 (1988) 135.
- [19] L.M. Pismen and J.D. Rodriguez, Mobility of singularities in the dissipative Ginzburg–Landau equation, *Phys. Rev. A* 42 (1990) 2471.
- [20] I. Aranson, H. Levine and L. Tsimring, Controlling spatiotemporal chaos, *Phys. Rev. Lett.* 72 (1994) 2561.
- [21] D. Meiron and A. Newell, The shape of stationary dislocations, *Phys. Lett. A* 113 (1985) 289.
- [22] A. Pocheau and V. Croquette, Dislocation motion: a wavenumber selection mechanism in Rayleigh–Bénard convection, *J. Phys. (Paris)* 45 (1984) 35; R. Ribotta and A. Joets, Defects and interaction with the structures in EHD convection in nematic liquid crystals, in: *Cellular Structures in Instabilities*, J.E. Weisfreid and S. Zaleski eds. (Springer, Berlin, 1984) p. 249; G. Goren, I. Procaccia, S. Rasenat and V. Steinberg, Interaction and dynamics of topological defects: theory and experiments near the onset of weak turbulence, *Phys. Rev. Lett.* 63 (1989) 1237.